

Dynamics of transient disordered vortex states in $\text{Bi}_2\text{Sr}_2\text{CaCu}_2\text{O}_{8+\delta}$

B. Kalisky, Y. Bruckental, A. Shaulov, and Y. Yeshurun

Institute of Superconductivity, Bar-Ilan University,

Ramat-Gan 52900, Israel

(July 23, 2003)

Abstract

The dynamics of transient disordered vortex states in $\text{Bi}_2\text{Sr}_2\text{CaCu}_2\text{O}_{8+\delta}$ was magneto-optically traced in three experiments: (i) during continuous injection of transient vortex states while ramping up the external magnetic field, (ii) during annealing of injected transient states while keeping the external field constant, and (iii) during annealing of transient 'supercooled' disordered states while ramping down the external field. The results reveal front-like propagation (experiment i) or retreat (experiments ii and iii) of the transient vortex states, at a rate governed by the rate of change of the external field, the annealing time τ of the transient states and the creep rate. The experimental results are theoretically analyzed in terms of competition between generation and annealing of transient disordered vortex states. Extraction of the annealing time τ from the above three experiments, yields the same results for τ as a function of the induction, B , and temperature T . Knowledge of $\tau(B, T)$ allows for correct determination of the thermodynamic order-disorder vortex phase transition line.

I. INTRODUCTION

The nature of the disorder-driven solid-solid vortex phase transition in high temperature superconductors has been an intriguing issue in physics of the vortex matter [1]. Recent studies have shown that proper characterization of this transition must take into account effects of transient disordered vortex states (TDVS) [2–13]. These transient states are inevitably created by injection of vortices through inhomogeneous surface barriers while the external magnetic field increases [2–4,11,14], or by "supercooling" of the disordered vortex phase while the field decreases [7,10,11,15]. The existence of such transient states is indicated in time resolved magneto-optical measurements by the appearance of a sharp change ('break') in the slope of the induction profiles [4,7]. When the external field is kept constant, the break moves with time towards the sample edges or center, indicating annealing of the injected or supercooled TDVS, respectively [4,11,12].

The existence of TDVS near the disorder-driven vortex phase transition, clarifies several long standing puzzles, such as the apparent increase of the transition induction with time [8,9,11–13], the apparent termination of the transition line below a certain temperature [11,12,19,22], yet the appearance of the transition over a longer time [11–13,19–22], and smearing of the first order nature of the transition [2,3]. Although some aspects of the TDVS have been analyzed [23,24], so far no comprehensive analysis of the dynamics of TDVS, and its influence on the measured transition, has yet been reported. At the experimental front, research efforts have been mainly directed towards eliminating the transient effects, e.g. by utilizing the Corbino disk configuration in transport measurements [2,3] and the vortex dithering technique in magnetic measurements [17]. These sophisticated experiments successfully uncovered the underlying thermodynamic order-disorder vortex phase transition. In this work we investigate, both experimentally and theoretically, the dynamics of the transient disordered vortex states, and utilize this knowledge to extract the thermodynamic order-disorder vortex phase transition line. We present comprehensive time resolved magneto-optical measurements in $\text{Bi}_2\text{Sr}_2\text{CaCu}_2\text{O}_{8+\delta}$ (BSCCO), demonstrating continuous injection of transient vortex states while ramping up the external magnetic field, annealing of injected transient states while keeping the external field constant, and annealing of transient 'supercooled' disordered states while ramping down the external field. In all these experiments the TDVS exhibit front-like propagation, or retreat, with a velocity depending on the rate of change of the external field, the creep rate and the annealing time τ of the transient states. The dynamic behavior of the front is quantitatively analyzed in terms of competition between two mechanisms, namely generation and annealing of TDVS. This analysis enables extraction of the annealing time τ , characterizing the TDVS, as a function of the induction B and temperature T . We show that knowledge of $\tau(T, B)$ enables the extraction of the thermodynamic vortex order-disorder transition line, $B_{od}(T)$. The extracted $B_{od}(T)$ line is significantly different from the apparent transition lines commonly measured from the onset of the second magnetization peak, ignoring effects of TDVS.

II. EXPERIMENTAL

Measurements were performed on a $1.55 \times 1.25 \times 0.05 \text{ mm}^3$ $\text{Bi}_2\text{Sr}_2\text{CaCu}_2\text{O}_{8+\delta}$ single crystal ($T_c = 92 \text{ K}$). The crystal was grown using the traveling solvent floating zone method [25].

This crystal was specially selected for its uniformity of flux penetration and was checked by magneto-optical imaging before and after it was cut into a rectangle. In the course of measurements, magneto optical (MO) snapshots of the induction distribution across the sample surface were recorded at time intervals of typically 40 ms, using iron-garnet MO indicator with in-plane anisotropy [26] and a high speed CCD camera (Hamamatsu C4880-80).

A. Field Sweep Up (FSU)

The process of injection of TDVS through the sample edges by sweeping up the external field, was magneto-optically recorded at different sweep rates. In these experiments, the sample was cooled down to the measuring temperature in zero field, then the external magnetic field, H_{ext} , was ramped up at a constant rate between 4 and 1600 G/sec, from zero to about 850 G. While the external magnetic field was ramped up, snapshots of the induction distribution across the crystal surface were taken successively at constant field intervals (usually 10 G).

Figure 1 shows the induction profiles across the crystal width deduced from the magneto-optical images, taken at $T = 23 K$, while the external field was ramped up at a rate of 53 G/sec. When H_{ext} reaches a value of approximately 430 G, a sharp change in the slope of the profile ("break") appears at $B_{f0} \simeq 360 G$, indicating coexistence of two distinct vortex states, characterized by high and low persistent current densities: A high persistent current state near the sample edges and a low persistent current state near the center [4]. The high persistent current state is identified as a TDVS, because it decays with time when the external field is kept constant (see Sec. IIB below). When the external field is continuously increased, the break moves towards the sample center, indicating propagation of the transient disordered state front deeper into the sample. At the same time, the induction at the break increases monotonically with a rate decreasing with time. As shown below (see Sec. IIIA), these results can be explained in terms of competition between injection and annealing processes of TDVS. While the rate of injection remains approximately constant, the rate of annealing is high for low inductions, and decreases sharply as the induction increases towards B_{od} . The first appearance of the break indicates a stage where the injection rate starts to overcome the annealing rate.

Increasing the field sweep rate, or decreasing temperature at a constant sweep rate, shifts B_{f0} downwards, indicating that the injection process of TDVS starts to overcome the annealing process at lower inductions. The effect of increasing sweep rate is demonstrated in Figure 2, which shows the induction profiles measured at $T = 25K$ while ramping up the external field at 4, 160, and 800 G/sec. A rate increase from 4 to 160 G/sec, shifts B_{f0} down from ~ 450 to ~ 400 G. A further increase of the rate to 800 G/sec shifts B_{f0} down to ~ 330 G. The effect of temperature on B_{f0} is demonstrated in Figure 3. For the same sweep rate of 160 G/sec, lowering temperature from 25 K to 23 K, shifts B_{f0} down from ~ 400 G to ~ 330 G. As temperature is further lowered to 21 K, B_{f0} is shifted down to ~ 200 G. Figure 4 shows the velocity of the TDVS front as a function of time for different sweep rates, measured at $T = 23 K$. The initial velocity of the front (the first appearing break) is zero. It then accelerates with a decreasing rate, approaching a constant velocity determined by the rate of change of the external field.

B. Annealing at a constant field

The annealing process of injected TDVS was magneto-optically recorded while keeping the external magnetic field at a constant level. Injection of TDVS throughout the sample was accomplished by abruptly raising the external field to a target value between 140 and 850 G (rise-time < 50 ms). Immediately after reaching the target value of the external field, magneto-optical snapshots of the induction distribution across the sample surface were recorded at time intervals of 40 ms for 4 seconds, and 300 ms for additional 26 seconds.

Figure 5 shows the time evolution of the induction profiles at $T = 21$ K after abruptly increasing the external field from zero to 465 G. Initially, the profiles are smooth, without a break, indicating a single vortex phase throughout the sample. However, after approximately 0.5 second, a break appears in the slope of the induction profiles, progressing with time towards the sample edge. The break, (a typical one is marked in the figure by an arrow), separates between a high persistent current state near the sample edge and a low persistent current state near the center. The high persistent current region near the edge shrinks with time, and therefore the vortex state in this region is identified as a transient disordered state. The vortex state in the expanding, low persistent current region near the center, is identified as the thermodynamic quasi-ordered phase [4]. The front of the growing thermodynamic phase moves initially with a large velocity and decelerates with time to zero velocity as shown in Figure 6, for $H_{ext} = 500$ and 625 G. After reaching zero velocity, the movement of the front reverses its direction, indicating an end of the annealing process and beginning of injection of TDVS into the sample interior. One would expect [4] that this turning point is obtained when the induction at the front reaches the value of the thermodynamic vortex order-disorder transition induction B_{od} . However, the data shows that the annealing process ceases at an induction of ~ 400 G, i.e. below $B_{od} = 430$ G (see Section IV).

We show below (Section IIIB), that the origin of this phenomenon is associated with the fundamental difficulty of realizing a 'pure' annealing experiment; While the external field is kept constant, disordered vortex states are continuously injected through the sample edges via flux creep. For inductions well below B_{od} the annealing rate is much larger, thus the thermodynamic quasi-ordered vortex state continuously grows. However, as the induction at the front approaches B_{od} , the annealing rate continuously decreases until a point is reached when the rate of injection of TDVS due to flux creep equals the annealing rate. At this point in time the growth of the thermodynamic quasi-ordered phase comes to an halt. After this point, the rate of injection of TDVS due to flux creep becomes larger than the annealing rate, and as a result TDVS are injected into the sample. This is manifested by the reverse movement of the front towards the sample center.

C. Field Sweep Down (FSD)

"Supercooling" of a disordered vortex phase [7] and annealing of the transient supercooled state were magneto-optically traced in field sweep down experiments. In these experiments, an external field of 850 G was initially applied for long enough time to ensure establishment of a disordered vortex phase. The field was then ramped down to zero at a constant rate between 4 and 1600 G/sec. While the external field was ramped down, snapshots of the

induction distribution across the crystal surface were taken successively at constant field intervals (usually 10 G). Figure 7 shows the induction profiles taken at $T = 23$ K, while the external field was ramped down at a rate of 16 G/sec. For external fields between 420 and 240 G the profiles exhibit a break, progressing into the sample interior with time. In contrast to FSU experiments, here the breaks appear at approximately the same induction, $B_f = 360$ G, almost independent of the location in the sample. As before, the breaks reveal coexistence of a quasi-ordered vortex phase (characterized by low persistent current density) near the sample edges, and a TDVS (characterized by high persistent current density), in the sample interior. The value of B_f is strongly suppressed by increasing the sweep rate at constant temperature or decreasing temperature at a constant sweep rate, as demonstrated in Figures 8 and 9, respectively. Obviously, in these experiments the source of the transient disordered state cannot be associated with edge contamination, as flux does not enter the sample through its edges. Moreover, the low j quasi-ordered phase appears near the edges and propagates with time into the sample interior. The origin of the TDVS is rather 'supercooling' of the high-field disordered state [7]. As the field is rapidly lowered below the transition field, the initial thermodynamically established disordered state is supercooled to inductions below B_{od} and consequently the apparent solid-solid transition induction, B_f , shifts below B_{od} . As shown in Figure 8, larger sweep-rates induce 'deeper' supercooling, shifting B_f further down [9].

Figure 10 describes the front velocity as a function of time in FSD experiments at 23 K, for different sweep rates. For low sweep rates, the front moves at an approximately constant velocity, which depends on the rate of change of the external field. For high sweep rates, the front movement accelerates with time.

III. THEORETICAL ANALYSIS

The experiments described above reveal different dynamic behaviors of the TDVS depending on the type of experiment (FSU, FSD or constant field), the rate of change of the external field, the induction at the interface between the TDVS and the quasi-ordered thermodynamic phase, temperature and time. In this section we analyze these behaviors in terms of a competition between two fundamental processes: creation and annealing of TDVS. The parameter that plays a key role in our analysis is the annealing time, τ , of the transient disordered vortex state. In defining τ , we refer to the annealing experiment described in Section IIB. We assume an initial TDVS throughout the whole sample, created, e.g. by a step increase of the external field. The annealing process begins at $t = 0$ with a nucleation of a quasi-ordered vortex phase at the sample center, and continues with front propagation of this phase towards the sample edges [4]. In order to distinguish between normal magnetic relaxation and the annealing process of the TDVS, we assume that the disordered and quasi-ordered vortex states are characterized by *time independent* high and low current densities, j_h and j_l , respectively. Such an idealized annealing process is schematically described in Figure 11a. Let us examine a location x in the sample where at $t = 0$ the induction is $B(x)$ and the current density is j_h . The annealing time, $\tau(B, T)$, is defined as the time that it takes for the current density at x to transform from j_h to j_l while the induction at x remains constant and equal to B [27]. Formally,

$$\tau(B, T) = t_N + \int_{\frac{d}{2}}^x \frac{dx}{v_f}, \quad (1)$$

where, t_N is the nucleation time, $v_f(B, T)$ is the front velocity under the conditions of constant external field H_{ext} and constant j_h and j_l ; $d/2$ denotes the location of the sample center, where the thermodynamic quasi-ordered vortex phase starts to nucleate [23]. According to Eq.1, $t_N = \tau(B_0)$, where B_0 is the induction at the sample center. Equation 1 provides insight into the qualitative behavior of $\tau(B)$: For low induction B , far below the transition induction B_{od} , v_f is large [4], resulting in a short annealing time τ . As B_{od} is approached, v_f decreases causing τ to increase. In a close vicinity of B_{od} , v_f approaches zero, and consequently τ approaches infinity.

In the following subsections we analyze the dynamics of the transient vortex states in the three experiments described in Section III and show how τ can be extracted from each of these experiments.

A. Field sweep up

In these experiments, two competing processes take place simultaneously: A TDVS is continuously injected into the sample through its edges by the ramped external field and flux creep, and at the same time the annealing process takes place. This competition between injection and annealing of the TDVS determines the position, x_f , of the front. In the framework of the critical state model, one can consider x_f as a function of three independent variables [28]: the external field, H_{ext} , the current density, j_h , and the induction, B_f , at the front (see Figure 12a):

$$x_f = (H_{ext} - B_f)/j_h. \quad (2)$$

Thus,

$$\frac{\partial x_f}{\partial t} = \frac{1}{j_h} \frac{dH_{ext}}{dt} - \frac{H_{ext} - B_f}{j_h^2} \left(\frac{\partial j_h}{\partial t} \right)_{H_{ext}, B_f} - \frac{1}{j_h} \left(\frac{\partial B_f}{\partial t} \right)_{H_{ext}, j_h}. \quad (3)$$

According to Eq. 1,

$$\left(\frac{\partial B_f}{\partial t} \right)_{H_{ext}, j_h} = \left(\frac{\partial B_f}{\partial x_f} \right) \left(\frac{\partial x_f}{\partial t} \right)_{H_{ext}, j_h} = j_h v_f = 1/(\partial\tau/\partial B)_{B=B_f}. \quad (4)$$

Thus,

$$\frac{\partial x_f}{\partial t} = \frac{1}{j_h} \frac{dH_{ext}}{dt} - x_f \frac{\partial}{\partial t} (\ln j_h) - \frac{1}{j_h (\partial\tau/\partial B)_{B=B_f}}. \quad (5)$$

The meaning of this equation is as follows: The first term on the right hand side describes a continuous injection of TDVS by the change of the external field, pushing the front of the injected TDVS from the sample edge towards the sample center at a rate determined by the

rate of change of H_{ext} (see figure 11b). The second term on the right hand side of Eq. 5 describes slow injection, in the same direction, caused by flux creep (note that $\frac{\partial}{\partial t}(\ln j_h) < 0$) (see figure 11c). The third term describes the annealing process, pushing the front in the *opposite* direction, i.e. towards the sample edge (see figure 11a). The competition between the above three terms determines the dynamics of the front. Initially, when H_{ext} starts to increase from a zero value, the inductions involved are far below B_{od} , and thus $\partial\tau/\partial B$ is small (for a schematic description of $\tau(B)$ see figure 13). As a result, the annealing term (third term on the right hand side of Eq. 5) dominates, and the TDVS has no chance to propagate into the sample, i.e. the front is stuck at the sample edge. As H_{ext} increases, the induction at the edge increases towards B_{od} , and the annealing term becomes less and less significant, because the annealing time τ , as well as $\partial\tau/\partial B$, continuously increase, approaching infinity as $B \rightarrow B_{od}$. Thus, the front starts its journey from the sample edge towards its center with a zero velocity, and accelerates with time towards a final velocity determined by the rate of change of the external field (neglect of the flux creep term in Eq. 5 is justified for large enough dH_{ext}/dt). We note that x_f may reach the sample center, and thus disappear, before this final velocity is obtained. Let us denote by B_{f0} the induction at the first detected front; Since $x_{f0} \approx 0$, substitution of $\partial x_f/\partial t = 0$ in Eq. 5 yields:

$$(\partial\tau/\partial B)_{B=B_{f0}} = \frac{1}{dH_{ext}/dt}. \quad (6)$$

Thus, measurements of B_{f0} for different rates of change of the external field yield $\partial\tau/\partial B$ as a function of B . On the basis of these data one can calculate τ as a function of B by integration:

$$\tau(B) = \int_0^B (\partial\tau/\partial B) dB. \quad (7)$$

Since $\partial\tau/\partial B$ increases monotonically as B_{od} is approached, Eq. 6 implies that B_{f0} is shifted down to lower inductions as dH_{ext}/dt increases, in accordance with the experiment (see Figures 2 and 14).

The time dependence of B_f can be analyzed by considering B_f as a function of H_{ext} , j_h , and x_f (see figure 12a):

$$B_f = H_{ext} - j_h x_f. \quad (8)$$

Thus:

$$\frac{\partial B_f}{\partial t} = \frac{dH_{ext}}{dt} - x_f \frac{\partial j_h}{\partial t} - j_h \frac{\partial x_f}{\partial t}. \quad (9)$$

When the front (indicated by a break in the profile) just appears: $x_f \approx 0$ and $\partial x_f/\partial t = 0$, thus $\partial B_f/\partial t = dH_{ext}/dt$, implying that $B_f(t)$ starts to rise at a rate equal to the rate of change of the external field. The second term on the right hand side of Eq. 9, $-x_f(\partial j_h/\partial t)$, also contributes to an increase of $\partial B_f/\partial t$ with time, however for large dH_{ext}/dt this contribution is negligible. The contribution of the third term, $-j_h(\partial x_f/\partial t)$, is much more significant and it causes a continuous decrease of $\partial B_f/\partial t$ with time down to zero, which is obtained when $\partial x_f/\partial t$ reaches its final value $(1/j_h)(dH_{ext}/dt)$ (see Eq. 5). Thus, the

increase of $\partial x_f/\partial t$ with time is translated into a decrease of $\partial B_f/\partial t$ with time. When flux injection due to flux creep is negligible, $\partial B_f/\partial t = 0$ for $B_f = B_{od}$. As noted before regarding x_f , B_f may disappear before reaching its saturated value B_{od} . In this case, the final value of B_f will be $H_{ext} - j_h d/2$.

B. Annealing at a constant field

For a constant H_{ext} , Equations 5 and 9 become

$$\frac{\partial x_f}{\partial t} = -x_f \frac{\partial}{\partial t} (\ln j_h) - \frac{1}{j_h (\partial\tau/\partial B)_{B=B_f}} \quad (10)$$

and

$$\frac{\partial B_f}{\partial t} = -x_f \frac{\partial j_h}{\partial t} - j_h \frac{\partial x_f}{\partial t}. \quad (11)$$

In the absence of injection by the change of the external field, injection by flux creep becomes significant. Thus, the terms $-x_f \frac{\partial}{\partial t} (\ln j_h)$ and $-x_f \frac{\partial j_h}{\partial t}$ in Eqs. 10 and 11, respectively, may not be neglected. Again, two competing processes may be recognized: injection of a TDVS by flux creep, pushing x_f towards the sample center, and annealing of the TDVS, pushing x_f towards the sample edge. Note that regarding B_f , both processes contribute to an increase of B_f with time. Assuming that initially $x_f = d/2$ and B_f is far below B_{od} , the second term on the right hand side of Eq.10 dominates (i.e. the annealing process dominates), and the front starts its journey towards the sample edge with a maximum velocity given by $-\frac{1}{j_h (\partial\tau/\partial B)_{B=B_f}}$. As x_f moves towards the sample edge, B_f increases, and consequently $(\partial\tau/\partial B)_{B=B_f}$ increases. Thus, the annealing process slows down, and x_f decelerates until $\partial x_f/\partial t = 0$. In the absence of the creep term in Eq. 10, $\partial x_f/\partial t = 0$ would imply $B_f = B_{od}$. Obviously, for B_f close to B_{od} , the injection by creep becomes significant and the first term on the right hand side of Eq. 10 must be taken into account. This implies that $\partial x_f/\partial t = 0$ at an induction B_{fm} smaller than B_{od} satisfying the equation:

$$-x_f \frac{\partial}{\partial t} (\ln j_h) = \frac{1}{j_h (\partial\tau/\partial B)_{B=B_{fm}}}. \quad (12)$$

When this condition is fulfilled, B_f continues to increase, beyond B_{fm} , at a rate $-x_f(\partial j_h/\partial t)$ due to the flux creep (see Eq. 11). For B_f larger than B_{fm} , the motion of the front reverses direction, i.e. $\partial x_f/\partial t > 0$, implying movement of the front towards the sample center.

C. Field sweep down

The key difference between field sweep down (FSD) and field sweep up (FSU) experiments is the source of the TDVS. Unlike FSU experiments, in FSD experiments the TDVS are not injected through the sample edges, but created by "supercooling" of a previously established

thermodynamic disordered vortex state. We assume that the ramping down of the external field begins at $t = 0$, from a large enough value, H_m , so that initially the entire induction profile in the sample is above B_{od} . Thus,

$$H_{ext}(t) = H_m - \left| \frac{dH_{ext}}{dt} \right| t, \quad (13)$$

and the vortices in the entire sample are in a thermodynamic disordered phase from $t = 0$ up to $t = t_{od}$,

$$t_{od} = \frac{H_m - B_{od}}{|dH_{ext}/dt|}, \quad (14)$$

when the induction at the sample edge equals B_{od} . For $t > t_{od}$, a supercooled TDVS begins to appear at the sample edge; as the external field continues to drop, the front of the supercooled transient states penetrates deeper into the sample. At the same time the annealing process takes place. Note that in contrast to the annealing experiments (Section IIIB), in FSD experiments the annealing process starts at the sample *edge*, where the induction is smallest, and thus the lifetime of the supercooled TDVS is shortest. Clearly, it will require infinitely long time to anneal the TDVS generated at the edge immediately after $t = t_{od}$. However, as the external field is ramped down, the induction at the edge drops, and consequently the annealing time continuously decreases. Thus, at a later time $t_{f0} > t_{od}$, the induction at the edge drops to $B_{f0} = B_{od} - |dH_{ext}/dt| (t_{f0} - t_{od})$, and consequently, the annealing time decreases to $\tau(B_{f0})$. A quasi-ordered vortex state (and thus the first front) will appear at the sample edge when

$$\tau(B_{f0}) = t_{f0} - t_{od} = \frac{B_{od} - B_{f0}}{|dH_{ext}/dt|}. \quad (15)$$

This condition defines B_{f0} at the crossing point of the straight line $(B_{od} - B)/|dH_{ext}/dt|$ plotted versus B , and the curve $\tau(B)$, (see Figure 13). From the shape of the $\tau(B)$ -curve it is clear that as $|dH_{ext}/dt|$ increases, this crossing point is shifted towards lower inductions B . This is in accordance with the experiment, which shows that as the ramping rate increases the induction at the first detected break in the induction profile is shifted down (see Figures 8 and 14). On the basis of Eq. 15, one can generate the τ vs. B curve by measuring B_{f0} for different ramping rates of the external field. We note, however, that in this case a pre-determination of B_{od} is required.

Once the front appears at the sample edge, its dynamics (i.e. x_f and B_f versus time) can be analyzed starting from an equation similar to Eq. 2 (see Figure 12b):

$$x_f = \frac{B_f - H_{ext}}{j_l}. \quad (16)$$

Using the same arguments as in the analysis of the FSU experiments, one obtains:

$$\frac{\partial x_f}{\partial t} = -\frac{1}{j_l} \frac{dH_{ext}}{dt} - x_f \frac{\partial}{\partial t} (\ln j_l) + \frac{1}{j_l} \frac{1}{(\partial\tau/\partial B)_{B=B_f}} \quad (17)$$

and

$$\frac{\partial B_f}{\partial t} = \frac{dH_{ext}}{dt} + x_f \frac{\partial j_l}{\partial t} + j_l \frac{\partial x_f}{\partial t}. \quad (18)$$

It is interesting to note that as far as x_f is concerned, in FSD experiments the three factors involved, namely ramping down of H_{ext} , flux creep, and the annealing, all push x_f in the same direction - towards the sample center. In contrast, the dynamics of B_f is governed by competing processes: both, ramping down of H_{ext} and flux creep push B_f downwards ($dH_{ext}/dt < 0$, and $\partial j_l/\partial t < 0$), while the annealing process shifts B_f upwards ($\partial x_f/\partial t > 0$). Thus, variations with time of x_f relative to B_f are much larger in FSD as compared to FSU experiments. This explains the outstanding qualitative difference between the induction profiles measured in FSD and FSU experiments, namely the apparent constancy of B_f in FSD experiments as compared to FSU experiments.

In order to follow the behavior of x_f and B_f with time, let us first ignore the contribution of flux creep (second term on the right hand sides of Eqs. 17 and 18). For relatively slow rate of change of H_{ext} , the first front appears at a relatively high induction, thus $(\partial\tau/\partial B)_{B=B_{f0}}$ is large, and the third term on the right hand side of Eq. 17 may be neglected compared to the first term. In this case $\partial x_f/\partial t \approx (-1/j_l)(dH_{ext}/dt)$. Thus, the initial velocity of the front is determined by the rate of change of the external field, in contrast to FSU experiment where the *final* velocity of the front is determined by dH_{ext}/dt . Furthermore, Eq. 18 implies that in this case $\partial B_f/\partial t \approx 0$, i.e., B_f is constant. The negative creep term in Eq. 18 causes slow decrease of B_f with time. According to Eq. 17, the slow decrease of B_f with time causes slow increase of $\partial x_f/\partial t$ with time. For high rate of change of H_{ext} , B_{f0} is small, and consequently $1/(\partial\tau/\partial B)_{B=B_{f0}}$ may not be neglected compared to dH_{ext}/dt . In this case, the term $(1/j_l)(1/(\partial\tau/\partial B)_{B=B_{f0}})$ contributes to increase the velocity of x_f . Similar contribution in the same direction is obtained from the creep term.

IV. DISCUSSION

The above analysis shows that the dynamics of TDVS is determined by the rate of change of the external field, the creep rate, and the rate of change with B of the annealing time $\tau(B)$. While the external field is changed at a constant rate, and the creep rate is slow, the annealing rate varies over a wide range, due to the strong dependence of τ on B . This dependence can be extracted from FSU and FSD experiments, using Eqs. 6 and 15, respectively, and can be measured directly from annealing experiments in the range of B where injection by creep can be neglected, as discussed in details in ref [12]. For the extraction of τ from FSU experiments, one only needs to measure B_{f0} for different sweeping rates of H_{ext} . The circles in Figure 14 show results of measurements of B_{f0} as a function of dH_{ext}/dt in FSU experiments conducted at $T = 23$ K. As predicted theoretically (see Section IIIA), B_{f0} decreases monotonically as dH_{ext}/dt increases. Results for $\tau(B)$ extracted from these data, using Eq. 6, are shown by the circles in Figure 15. The solid line in this figure shows a theoretical fit to the Eq.

$$\tau = \frac{\tau_0}{(1 - \frac{B}{B_{od}})^\gamma}. \quad (19)$$

Evidently, a good fit is obtained over a wide range down to $B = 200 G$. The fit yields $\tau_0 = 0.011 s$, $\gamma = 2.6$ and $B_{od} = 460 G$. This value of B_{od} is used for the extraction of $\tau(B)$ from FSD experiments. The squares in Figure 14 show B_{f0} as a function of dH_{ext}/dt in FSD experiments at the same temperature. Interestingly, one observes that the values of B_{f0} in FSU (circles) and FSD (squares) experiments are similar. Note that for $\gamma = 1$ in Eq. 19, Eqs. 6 and 15 predict the same values of B_{f0} for both experiments for a given dH_{ext}/dt . For $\gamma > 1$, these equations predict higher values of B_{f0} for FSD experiments [29], as observed experimentally. The bold squares in Fig. 15 show $\tau(B)$ as extracted from FSD experiments using Eq. 15. Evidently, these results are in a very good agreement with the results of measurements of $\tau(B)$ from FSU experiments (circles in Fig. 15). The triangles in Fig. 15 depict direct measurements of $\tau(B)$ from annealing experiments [12]. Good agreement with the previous results is obtained over a wide range of inductions. Deviations are expected for larger inductions, where injection of TDVS by creep becomes significant.

Measurements of $\tau(B)$ at different temperatures are shown in Figure 16. Evidently, the lifetime spectrum of the TDVS widens as temperature is lowered [11]. Fits of these data to Eq. 19, yields $\tau_0(T)$ and the thermodynamic transition line $B_{od}(T)$. In Figure 17 we show the temperature dependence of B_{od} as extracted by this method. For comparison, we also show non-equilibrium transition lines [11] (dashed curves) as measured by the onset of the second magnetization peak, for different sweeping rates of the external field. It is seen that deviations from the thermodynamic transition line increase with increasing sweeping rates. Direct measurement of the thermodynamic transition line would require measurements at extremely low rates to allow for complete annealing of the TDVS. Alternatively, one can determine $B_{od}(T)$ indirectly from Eq. 19, by measuring $\tau(B, T)$ as outlined above.

Figure 18 shows the temperature dependence of τ_0 as obtained from the theoretical fits of the data of Fig. 16 to Eq. 19. Apparently, τ_0 increases exponentially as the temperature is lowered. The solid line in this figure is a fit of $\tau_0(T)$ to Arrhenius law: $8 \times 10^{-9} \exp(326/T)$. The exponential increase of τ_0 as temperature is lowered explains the disappearance of the second magnetization peak at low temperature, which was misinterpreted as termination of the transition line [11,12,19,22].

Once the functional dependence of τ on B is known, one can test the predictions of the above analysis for the velocity $\partial x_f / \partial t$ of the interface between the quasi-ordered phase and the TDVS, in the three experiments described above. The solid curves in Figures 4 and 10 are calculated from Eqs. 5 and 17 using the measured values of $j_h(t)$, $j_l(t)$ and B_{f0} . A fairly good agreement with the experimental data is obtained using $B_{od} = 480 G$.

A totally different behavior of $\partial x_f / \partial t$ is obtained in annealing experiments. As described in Section IIB, in this case the initial velocity is high, it gradually drops to zero at an induction below B_{od} , and then reverses direction (see Figure 6). The analysis outlined above (see Section IIIB) is capable of predicting this behavior as shown by the solid curve in Figure 6. This curve was calculated taking into account both, the annealing term and the creep term in Eq. 10. A reasonable agreement with the experimental data is obtained using the same value of B_{od} , and $\tau_0 = 0.04 s$.

V. SUMMARY AND CONCLUSIONS

We have visually traced the processes of generation and annealing of TDVS, using a high-speed magneto-optical system. Snapshots of the induction distribution reveal front-like propagation or retreat of the transient disordered states. The velocity of this front is governed by the rate of change of the external field, the induction at the front, temperature and time. We analyzed the dynamics of the front, in three different experiments, in terms of competition between creation and annealing of TDVS, where the annealing process is governed the annealing time $\tau(B, T)$. The predictions of this analysis are in good agreement with the experimental results. In particular, extraction of the annealing time $\tau(B, T)$ from the three experiments, yield the same results. The exponential increase of $\tau(B)$ with decreasing temperature, explains broadening of the second magnetization peak and its disappearance below a certain temperature [11,12,19,22] - a phenomenon that was misinterpreted as termination of the transition line. Reliable measurement of the thermodynamic order-disorder transition line $B_{od}(T)$ requires magnetic measurements at extremely low field sweep rates to allow for complete annealing of the transient states. This requirement becomes more severe as the temperature is lowered, because of the exponential increase of the annealing time. The thermodynamic transition line, $B_{od}(T)$, can be indirectly determined by fitting τ to Eq. 19. Measurement of the transition line in this method yields results which are significantly different from the non-equilibrium transition lines, commonly measured from the onset of the second magnetization peak, neglecting effects of transient vortex states.

VI. ACKNOWLEDGEMENTS

We thank Tsuyoshi Tamegai for providing us with the $\text{Bi}_2\text{Sr}_2\text{CaCu}_2\text{O}_{8+\delta}$ crystal. A.S. acknowledges support from the German-Israel Foundation (GIF). Y.Y. acknowledges support from the ISF Center of Excellence Program, by the Heinrich Hertz Minerva Center for High Temperature Superconductivity, and by the Wolfson Foundation.

REFERENCES

- [1] B. Khaykovich, E. Zeldov, D. Majer, T.W. Li, P.H. Kes, and M. Konczykowski, *Phys. Rev. Lett.* **76**, 2555 (1996); R. Cubitt, E.M. Forgan, G. Yang, S.L. Lee, D.M. Paul, H.A. Mook, M. Yethiraj, P.H. Kes, T.W. Li, A.A. Menovsky, Z. Tarnawski, and K. Mortensen, *Nature* **365**, 407 (1993); S.L. Lee, P. Zimmermann, H. Keller, M. Warden, R. Schauwecker, D. Zech, R. Cubitt, E.M. Forgan, P.H. Kes, T.W. Li, A.A. Menovsky, and Z. Tarnawski, *Phys. Rev. Lett.* **71**, 3862 (1993); D. Giller, A. Shaulov, Y. Yeshurun, and J. Giapintzakis, *Phys. Rev. B* **60**, 106 (1999); Y. Radzyner, A. Shaulov, and Y. Yeshurun, *Phys. Rev. B* **65** R100513.
- [2] Y. Paltiel, E. Zeldov, Y. N. Myasoedov, H. Shtrikman, S. Bhattacharya, M. J. Higgins, Z. L. Xiao, E. Y. Andrei, P. L. Gammel, and D. J. Bishop, *Nature* **403**, 398 (2000).
- [3] Y. Paltiel, E. Zeldov, Y. Myasoedov, M. L. Rappaport, G. Jung, S. Bhattacharya, M. J. Higgins, Z. L. Xiao, E. Y. Andrei, P. L. Gammel and D. J. Bishop, *Phys. Rev. Lett.* **85**, 3712 (2000).
- [4] D. Giller, A. Shaulov, T. Tamegai, and Y. Yeshurun, *Phys. Rev. Lett.* **84**, 3698 (2000).
- [5] E. Y. Andrei, Z. L. Xiao, W. Henderson, Y. Paltiel, E. Zeldov, M. Higgins, S. Bhattacharya, P. Shuk, and M. Greenblatt, *Condensed Matter Theories* **16**, 241 (2001).
- [6] D. Giller, B. Kalisky, A. Shaulov, and Y. Yeshurun, *J. Appl. Phys.* **89**, 7481 (2001).
- [7] C. J. van der Beek, S. Colson, M. V. Indenbom, M. Konczykowski, *Phys. Rev. Lett.* **84** 4196 (2000).
- [8] M. Konczykowski, C. J. van der Beek, S. Colson, M. V. Indenbom, P. H. Kes, Y. Paltiel, E. Zeldov, *Physica C* **341**, 1317 (2000).
- [9] H. Kupfer, A. Will, R. Meier-Hirmer, T. Wolf, A. A. Zhukov, *Phys. Rev. B.* **63**, 214521 (2001).
- [10] D. Giller, A. Shaulov, L. Dorosinskii, T. Tamegai, and Y. Yeshurun, *Physica C* **341**, 987 (2000).
- [11] B. Kalisky, D. Giller, A. Shaulov, and Y. Yeshurun, *Phys. Rev. B* **67**, R140508 (2003).
- [12] B. Kalisky, A. Shaulov, and Y. Yeshurun, *Phys. Rev. B* **68**, 012502 (2003).
- [13] B. Kalisky, A. Shaulov, T. Tamegai, and Y. Yeshurun, *J. Appl. Phys.* **93**, 8659 (2003).
- [14] B. Kalisky, Y. Wolfus, A. Shaulov and Y. Yeshurun, *Physica C*, **388**, 737, (2003).
- [15] B. Kalisky, A. Shaulov and Y. Yeshurun, *Physica C*, **388**, 695, (2003).
- [16] D. Giller, B. Kalisky, I. Shapiro, B. Ya. Shapiro, A. Shaulov and Y. Yeshurun, *Physica C*, **388**, 731. (2003).
- [17] N. Avraham, B. Khaykovich, Y. Myasoedov, M. Rappaport, H. Shtrikman, D. E. Feldman, T. Tamegai, P. H. Kes, M. Li, M. Konczykowski, K. van der Beek, E. Zeldov, *Nature* **411**, 451 (2001).
- [18] B. Khaykovich, E. Zeldov, D. Majer, T. W. Li, P. H. Kes, and M. Konczykowski, *Phys. Rev. Lett.* **76**, 2555 (1996).
- [19] Y. Yeshurun, N. Bontemps, L. Burlachkov and A. Kapitulnik, *Phys. Rev. B* **49**, R1548 (1994).
- [20] T. Tamegai, Y. Iye, I. Oguro, and K. Kishio, *Physica C* **213**, 33 (1993).
- [21] S. Anders, R. Parthasarathy, H. M. Jaeger, P. Guptasarma, D.G. Hinks and R. van Veen, *Phys. Rev. B* **58**, 6639 (1998).
- [22] S. Li and H. Wen, *Phys. Rev. B* **65**, 214515 (2002).

- [23] D. Giller, B. Ya. Shapiro, I. Shapiro, A. Shaulov and Y. Yeshurun Phys. Rev. B **63**, R220502 (2001).
- [24] M. V. Indenbom, E. H. Brandt, C. J. van der Beek and M. Konczykowski, cond-mat/0208468 v1 (2002).
- [25] N. Motohira *et al.*, J. Ceram. Soc. Jpn. **97**, 994 (1989).
- [26] V. K. Vlasko-Vlasov *et al.*, in Physics and Materials Science of Vortex States, Flux Pinning and Dynamics, edited by R. Kossowsky *et al.*, NATO ASI, Ser. E, Vol. **356** (Kluwer, Kordrecht, 1999), p. 205.
- [27] Our definition of τ may imply dependence of τ on the location x . However, measurements of τ at different locations in BSCCO samples [11] show only minor variations in τ at different locations with the same B .
- [28] Our analysis strictly applies to the parallel geometry where demagnetization effects are absent. Including these effects for the perpendicular geometry is not expected to change the overall physical picture of competition between injection and annealing: Obviously, the annealing process will not be affected, as it is governed by $\tau(B)$; For the injection process, the role of dH_{ext}/dt will be played by dB_{edge}/dt .
- [29] Eqs. 6, 15 and 19 yield: $(B_{od} - B_{f0}^{FSU})/(B_{od} - B_{f0}^{FSD}) = \gamma^{\frac{1}{1+\gamma}}$.

Figure captions

Figure 1. Induction profiles across a BSCCO crystal measured at $T = 23$ K, while ramping the external field at a rate of 53 G/sec. Note the sharp change in the slope of the profiles ("break") appearing for $H_{ext} > 430$ G. Bold lines represent profiles with and without (shorter times) break.

Figure 2. Induction profiles measured at $T = 25$ K while ramping the external field at different rates. As dH_{ext}/dt increases, the first break in the profiles appears at a lower induction.

Figure 3. Induction profiles measured at different temperatures, while ramping the external field at the same rate. As temperature is lowered, the first break in the profiles appears at a lower induction.

Figure 4. Velocity of the penetrating front of the transient disordered state as a function of time for different sweep rates of the external field. Solid lines are calculated from Eq. 3.

Figure 5. Time evolution of the induction profiles after abruptly increasing the external field from zero to 465 G. At approximately $t = 0.5$ s, a sharp change (a 'break') in the slope of the profiles appears, progressing with time towards the sample edge.

Figure 6. Velocity of the propagating front of the quasi-ordered vortex phase as a function of time for $H_{ext} = 500$ and 625 G. Note that the movement of the front reverses its direction, indicating an end of the annealing process and beginning of injection of transient disorder vortex state by flux creep. Solid lines are calculated from Eq. 10.

Figure 7. Induction profiles measured at $T = 23$ K, while the external field was ramped down at a rate of 16 G/sec. For external fields between 420 and 240 G the profiles exhibit a break, progressing into the sample interior with time. Bold lines represent profiles with and without (longer times) break.

Figure 8. Induction profiles measured at $T = 25$ K while ramping down the external field at different rates. As $|dH_{ext}/dt|$ increases, the breaks in the profiles appear at lower inductions.

Figure 9. Induction profiles measured at $T = 25\text{ K}$ and $T = 30\text{ K}$ while ramping down the external field at 160 G/sec . As temperature decreases, the breaks in the profiles appear at lower inductions.

Figure 10. Velocity of the quasi-ordered phase front as a function of time in field sweep down experiments, for different sweep rates. Solid curves are calculated from Eq. 17.

Figure 11. Schematic induction profiles illustrating motion of the interface between the quasi-ordered phase and the transient disordered state due to changes with time of the induction B_f (a), the external field (b), and the current density j_h (c). Diagram (a) illustrates an 'ideal' annealing process.

Figure 12. Schematic induction profile illustrating the relationship between the external field H_{ext} , the induction B_f at the break, the current density j_h of the transient disordered state, and the location x_f of the interface between the quasi-ordered phase and the transient disordered state, for field-sweep-up (a) and field-sweep-down (b).

Figure 13. Graphic procedure for determination of the induction B_{f0} at the first detected interface between the quasi-ordered phase and the transient disordered state, in field sweep down experiments: B_{f0} is the crossing point of the straight line $(B_{od} - B)/(dH_{ext}/dt)$ plotted versus B , and the curve $\tau(B)$.

Figure 14. Measurements of B_{f0} as a function of dH_{ext}/dt in field sweep up (circles) and field sweep down (squares) experiments conducted at $T = 23\text{ K}$.

Figure 15. Measurements of the annealing time τ as a function of B from field sweep up (circles), field sweep down (squares) and annealing (triangles) experiments. The solid line is a theoretical fit.

Figure 16. Measurements of the annealing time $\tau(B)$ at different temperatures.

Figure 17. The thermodynamic transition line $B_{od}(T)$ (continuous curve) as obtained from theoretical fit of the data of Fig. 15 to Eq. 19. For comparison, non-equilibrium transition lines, measured from the onset of the second magnetization peak for different field sweep rates, are shown by the dashed lines.

Figure 18. $\tau_0(T)$ as obtained from theoretical fit of the data of Fig. 15 to Eq. 19.

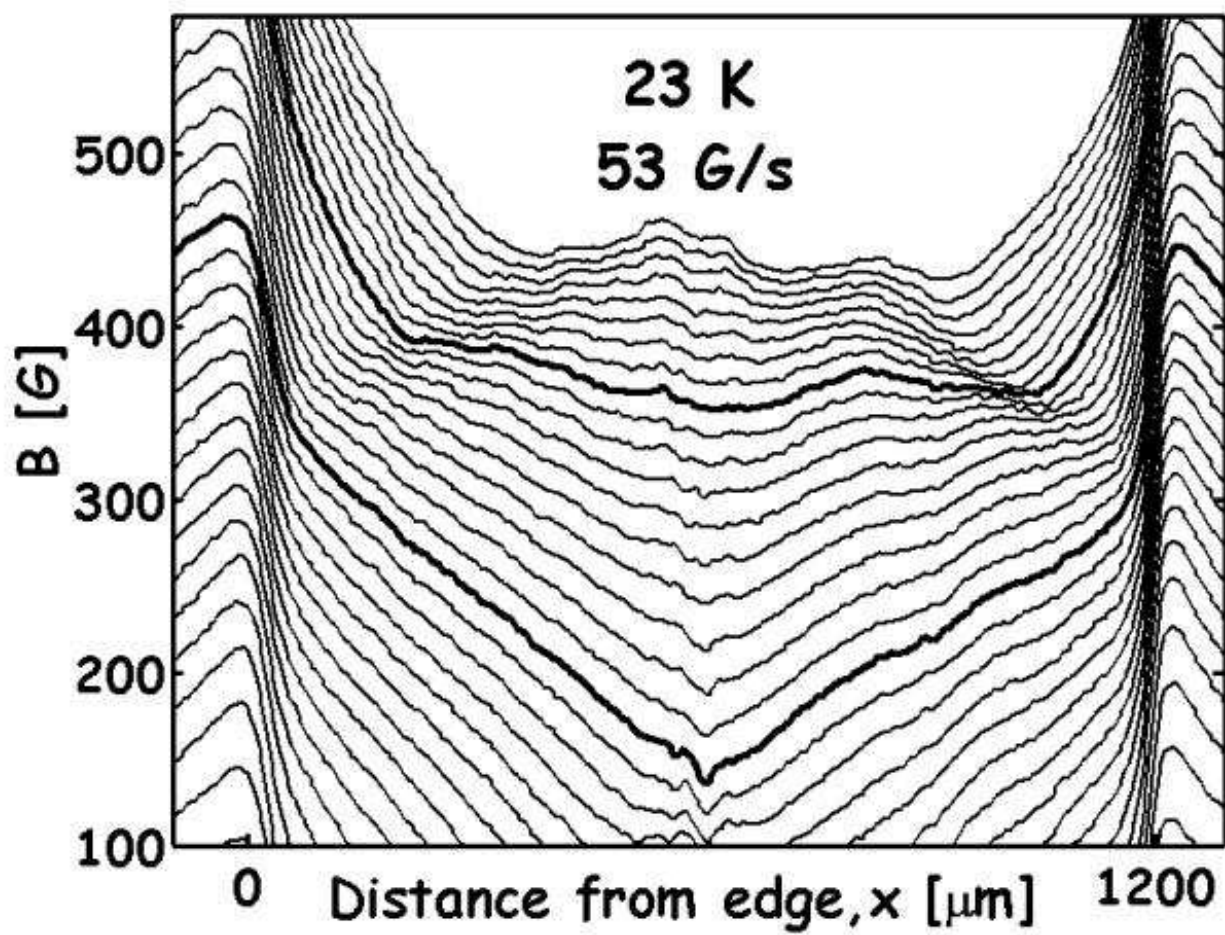


Figure 1 Kalisky *et al.*

$T = 25 \text{ K}$

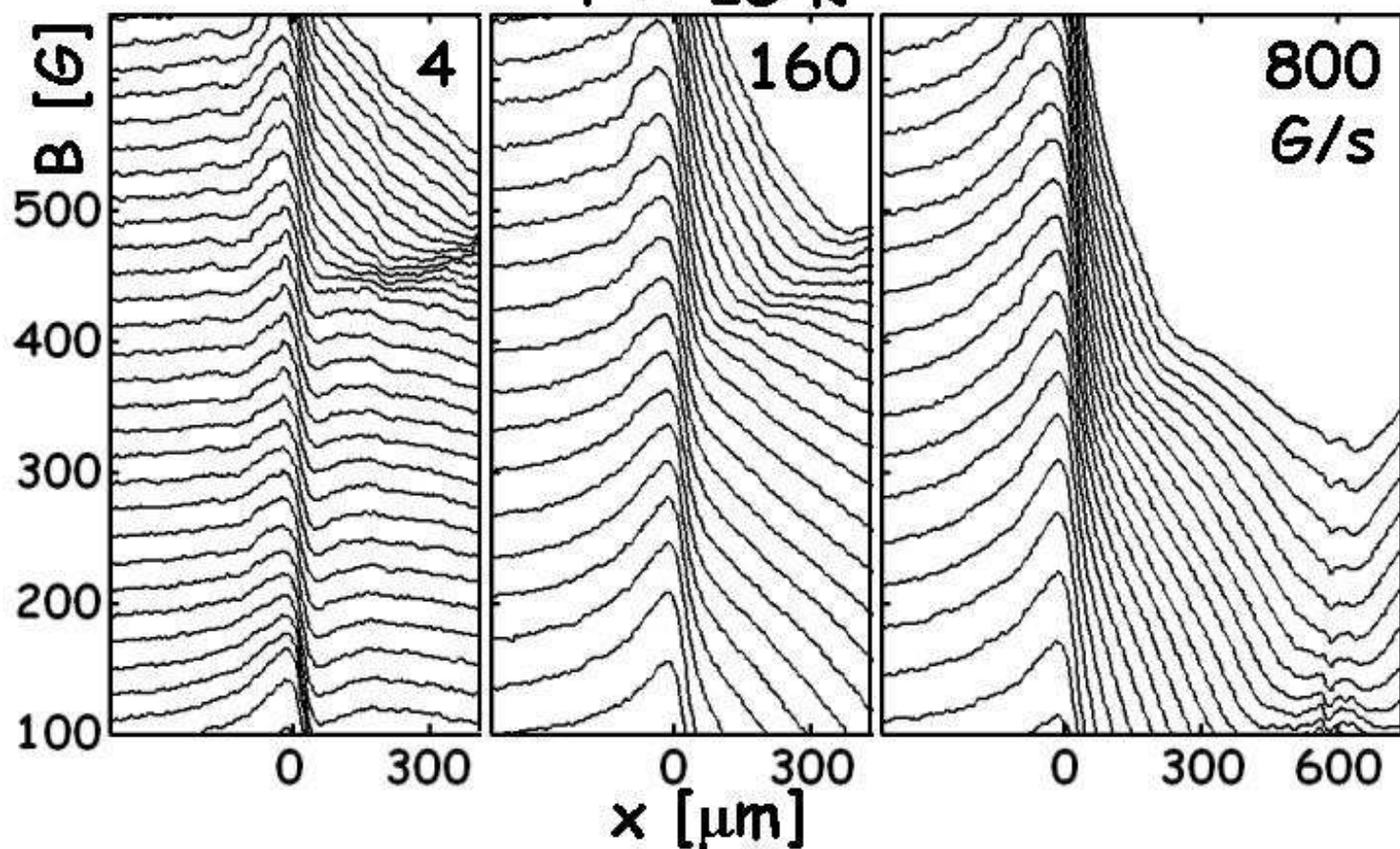


Figure 2 Kalisky *et al.*

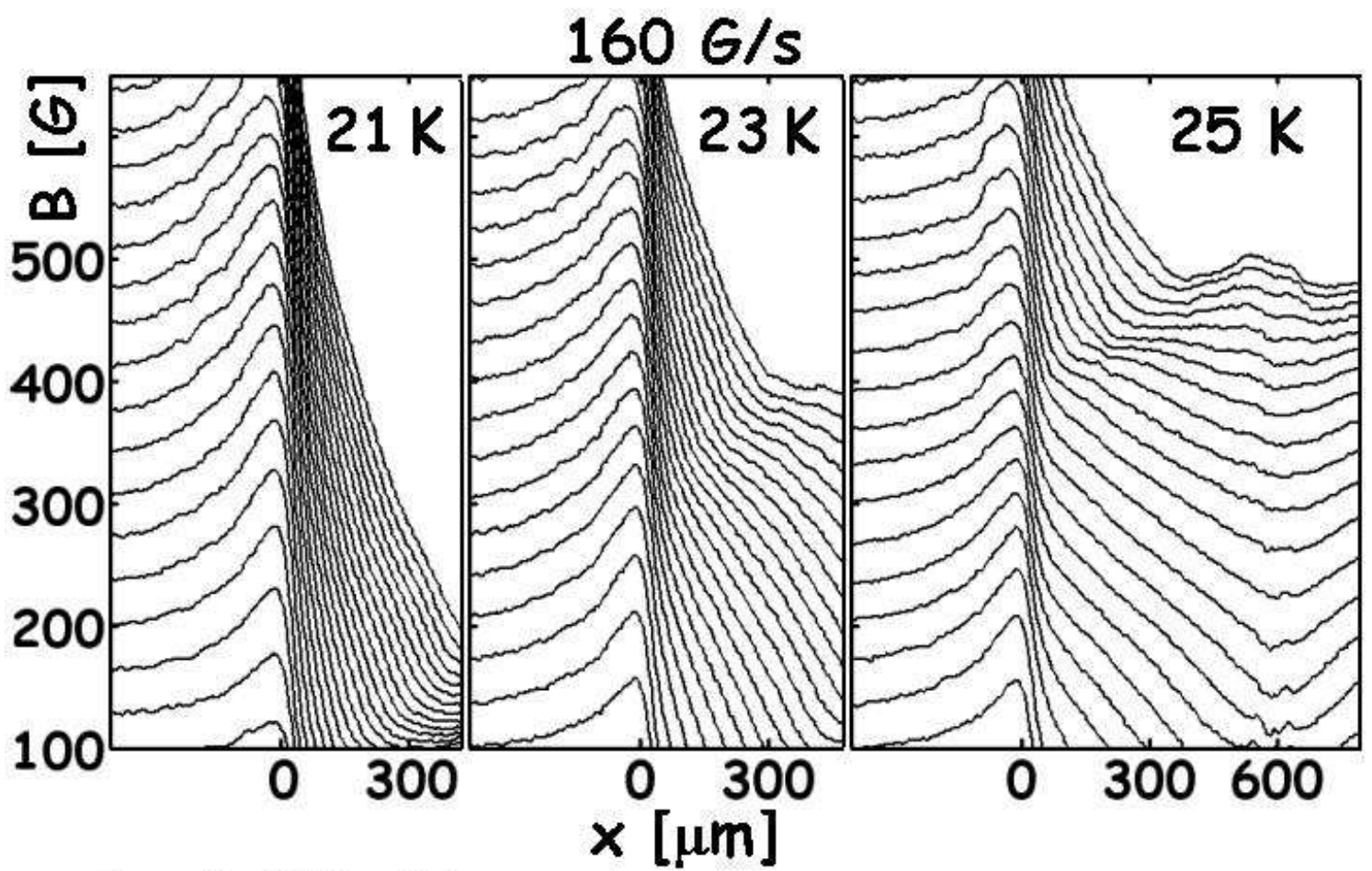


Figure 3 Kalisky *et al.*

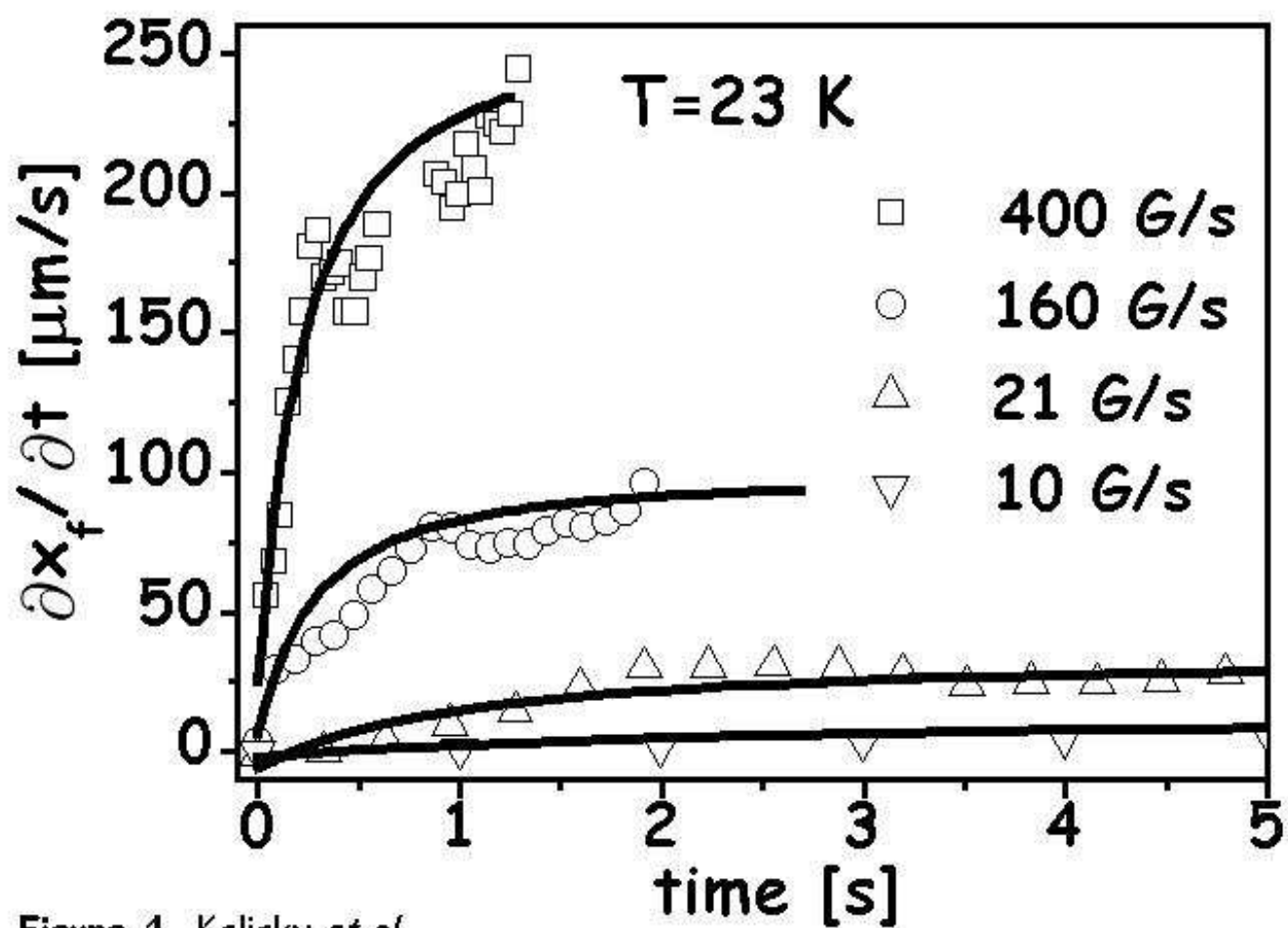


Figure 4 Kalisky *et al.*

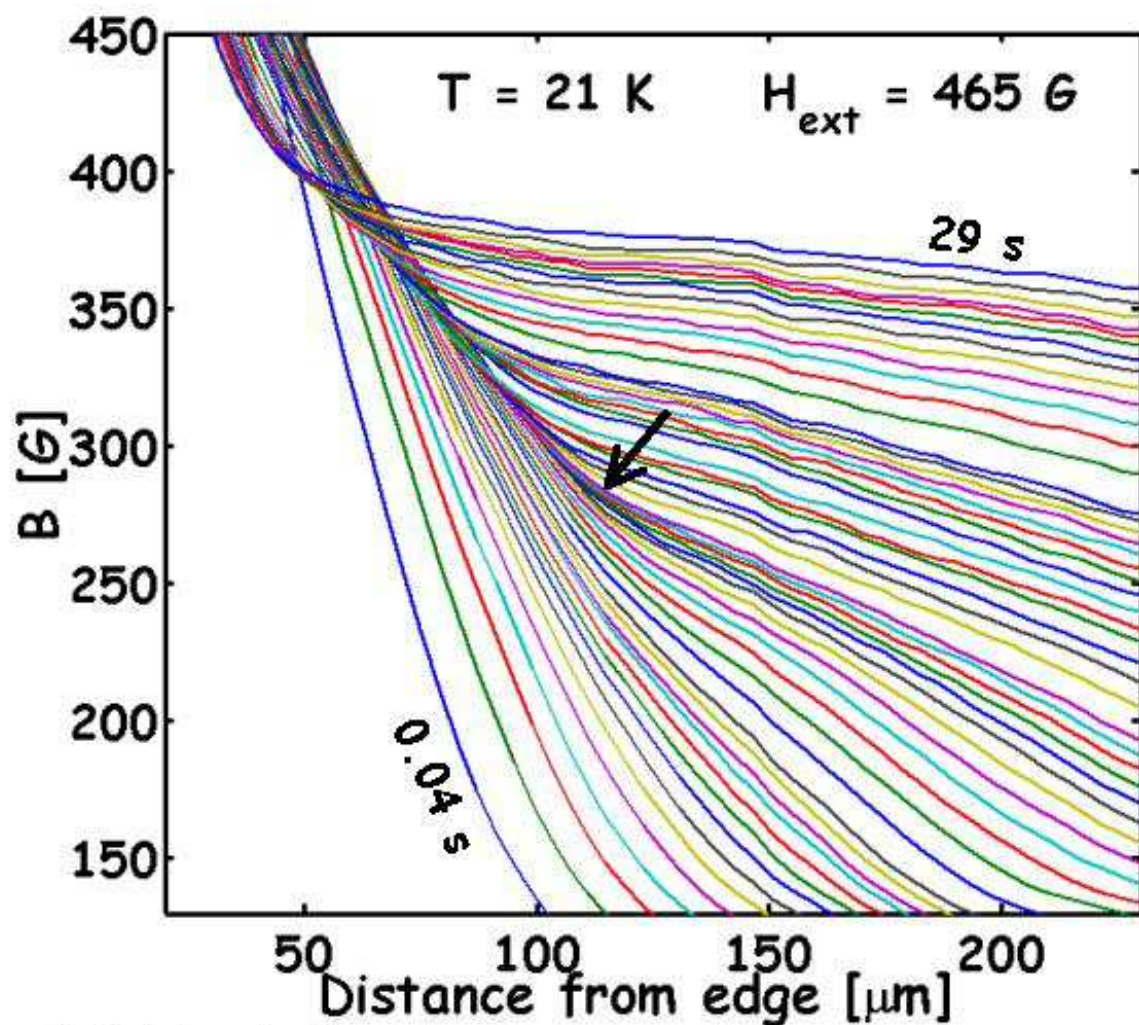


Figure 5 Kalisky *et al.*

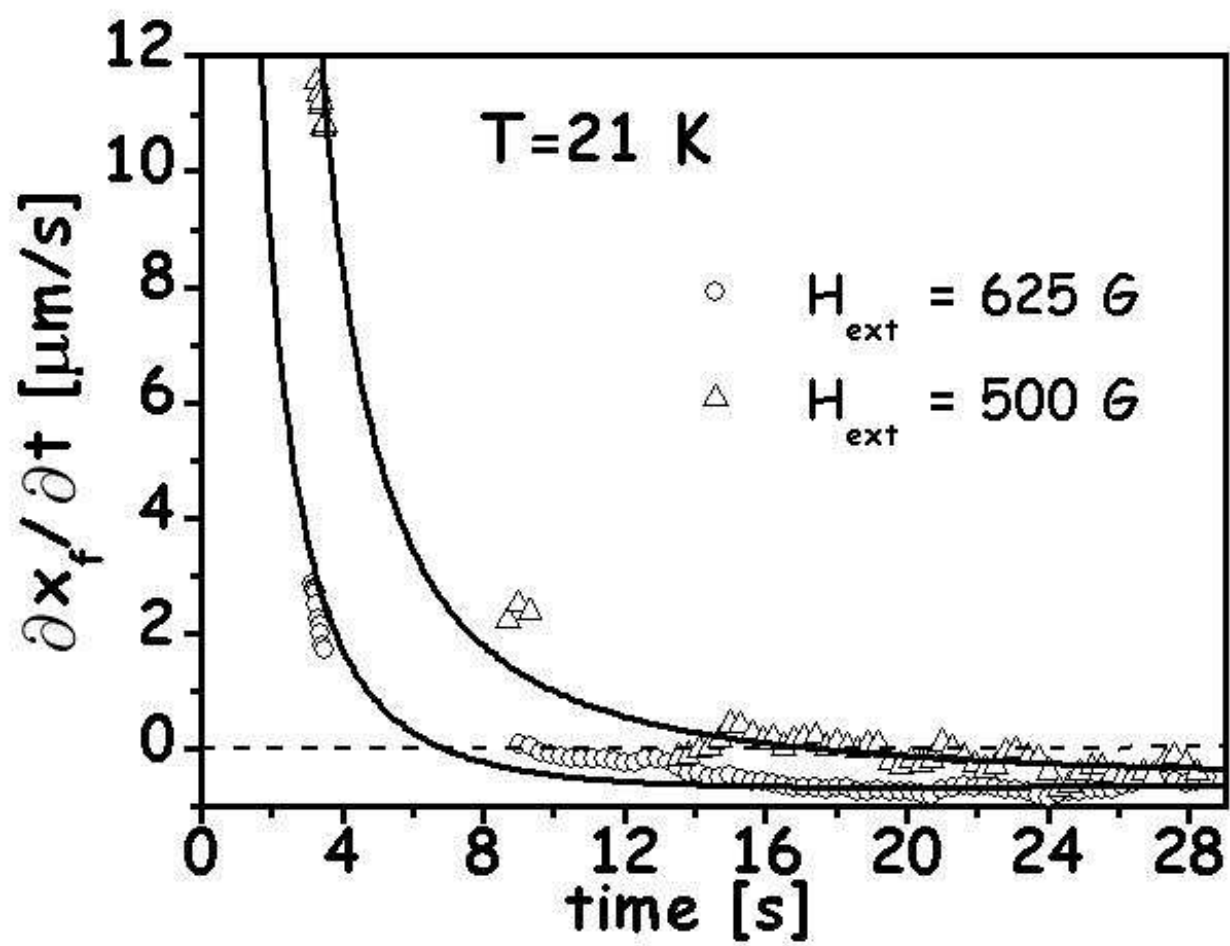


Figure 6 Kalisky *et al.*

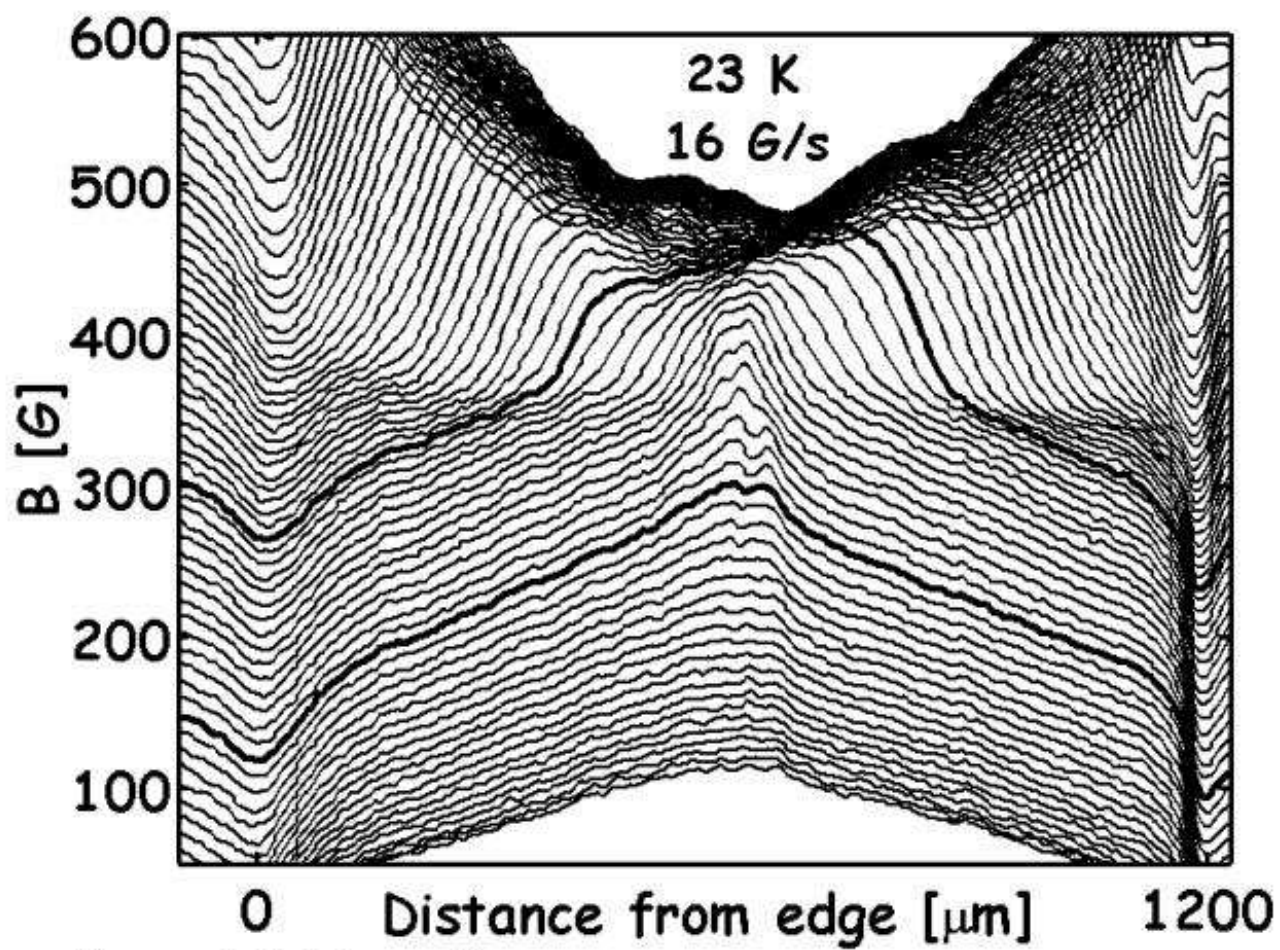


Figure 7 Kalisky *et al.*

T = 25 K

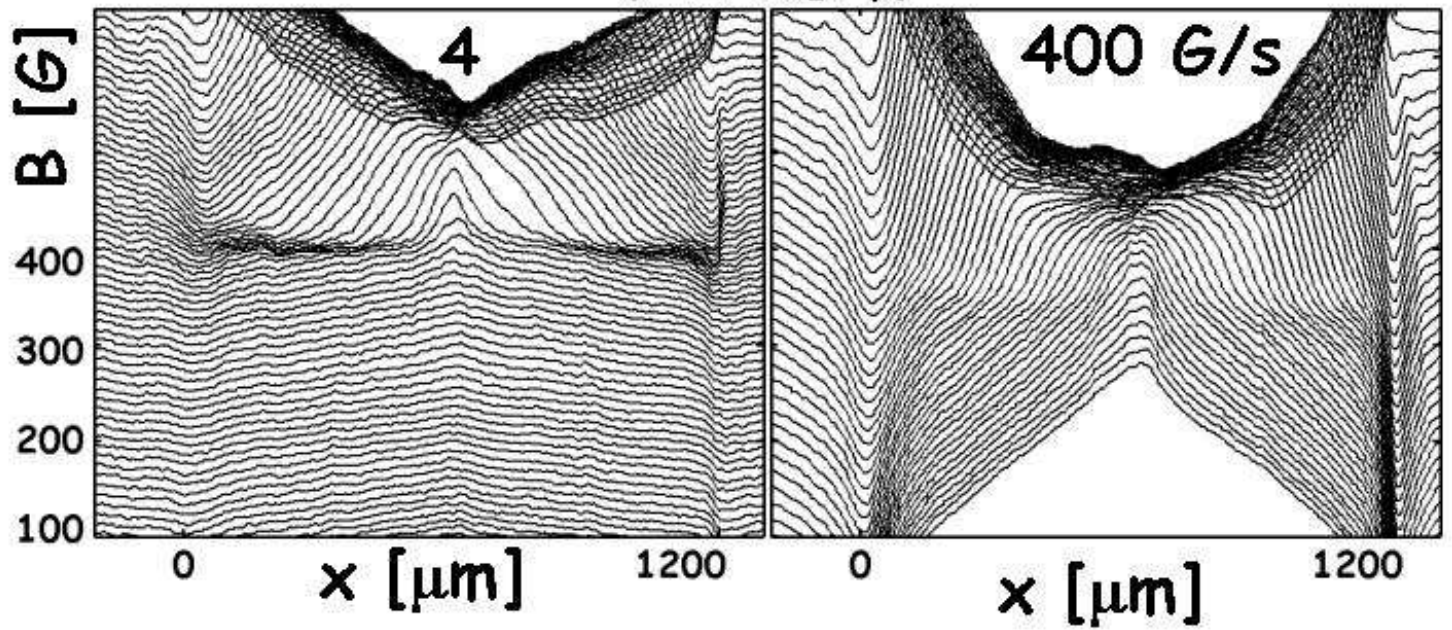


Figure 8 Kalisky *et al.*

160 G/s

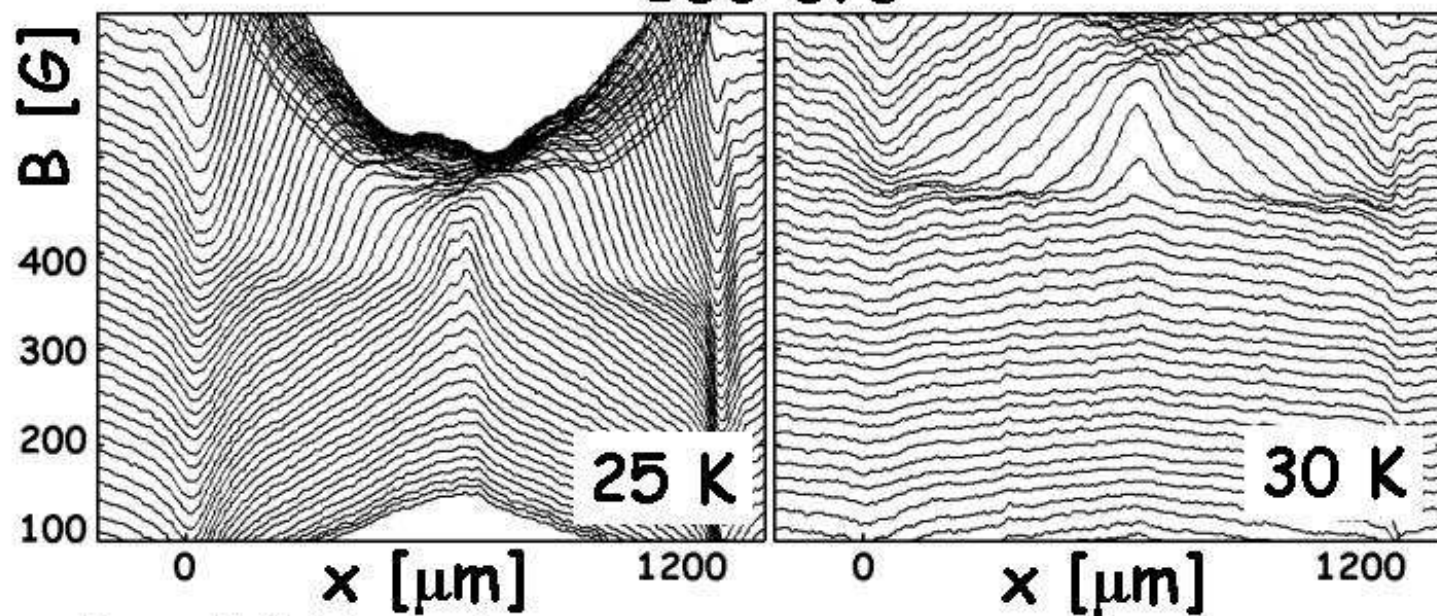


Figure 9 Kalisky *et al.*

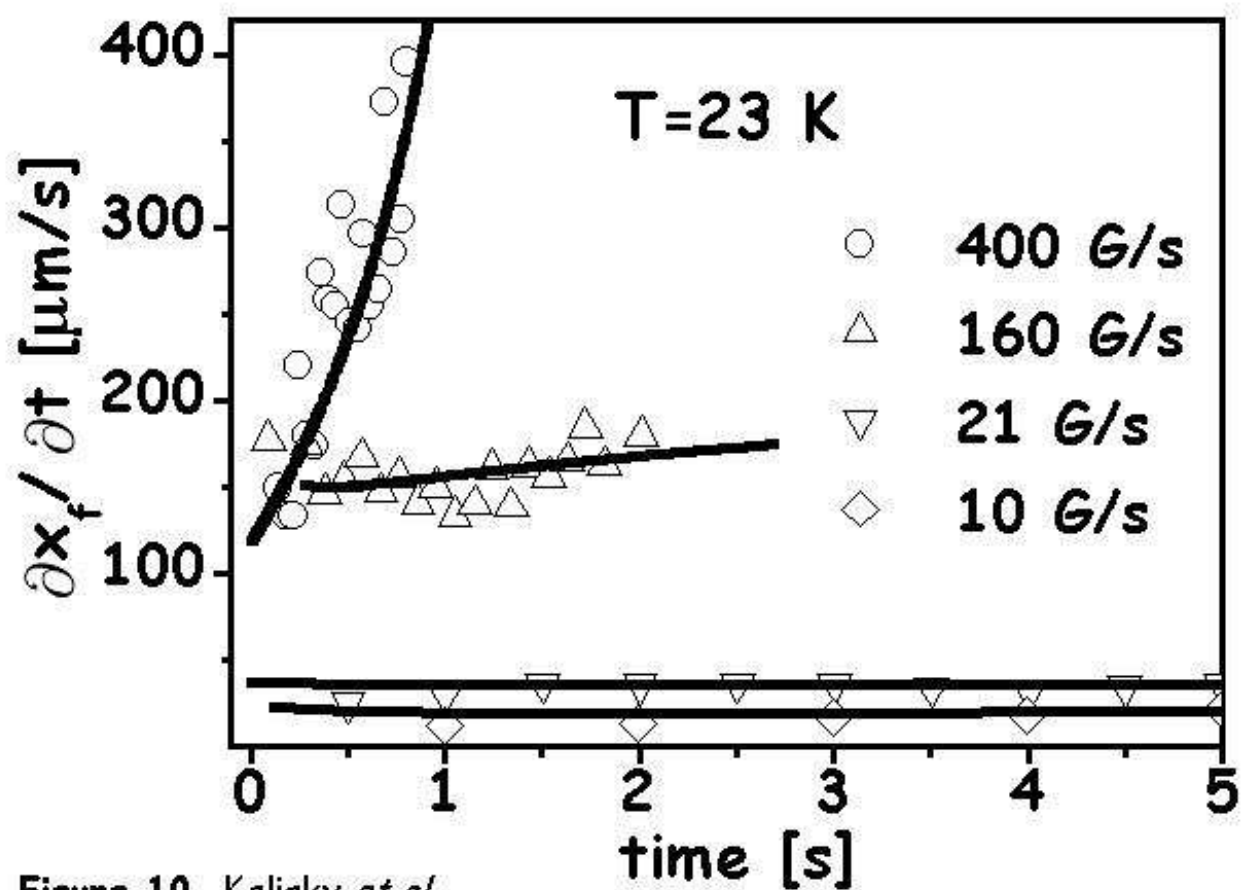


Figure 10 Kalisky *et al.*

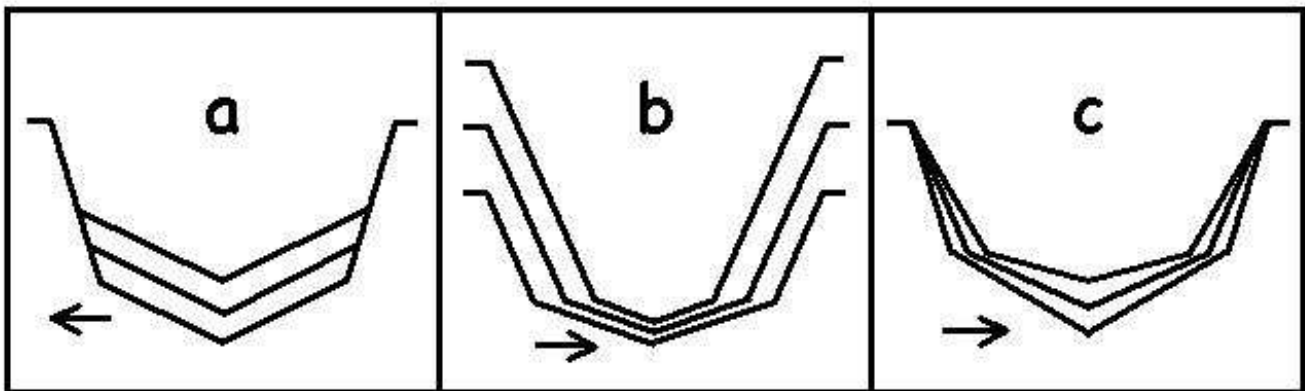


Figure 11 Kalisky *et al.*

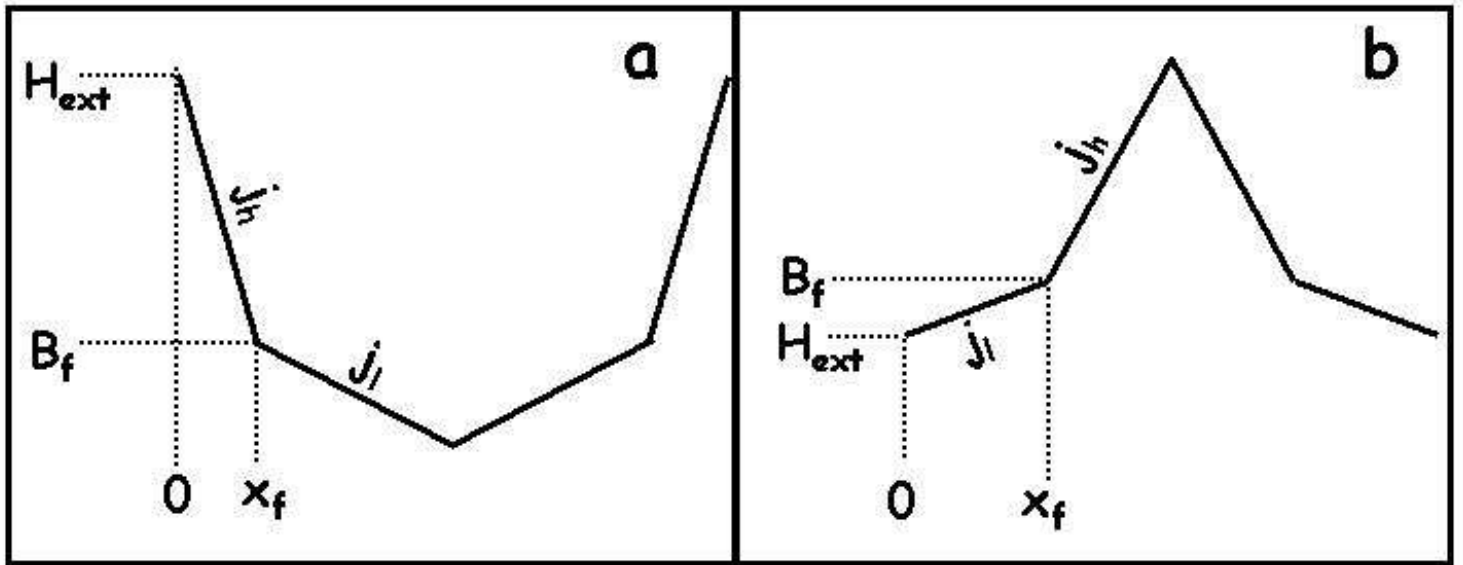


Figure 12 Kalisky *et al.*

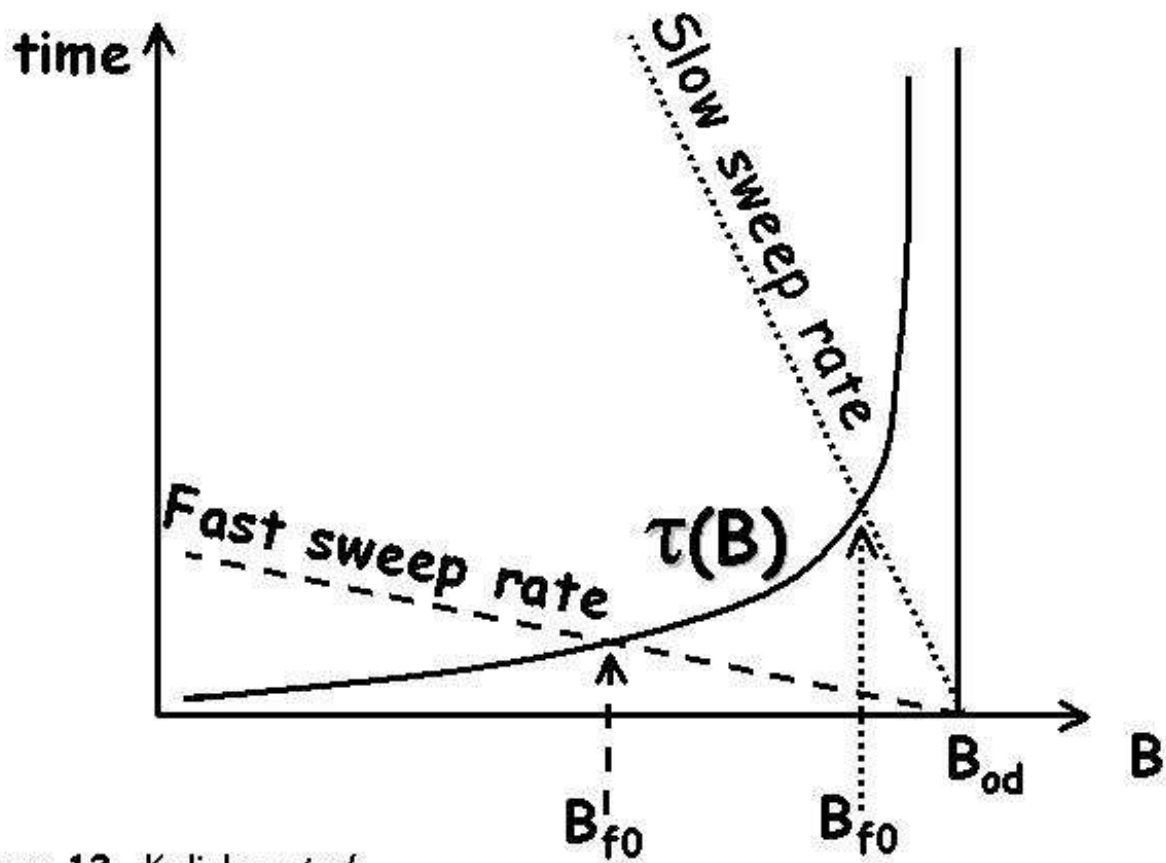


Figure 13 Kalisky *et al.*

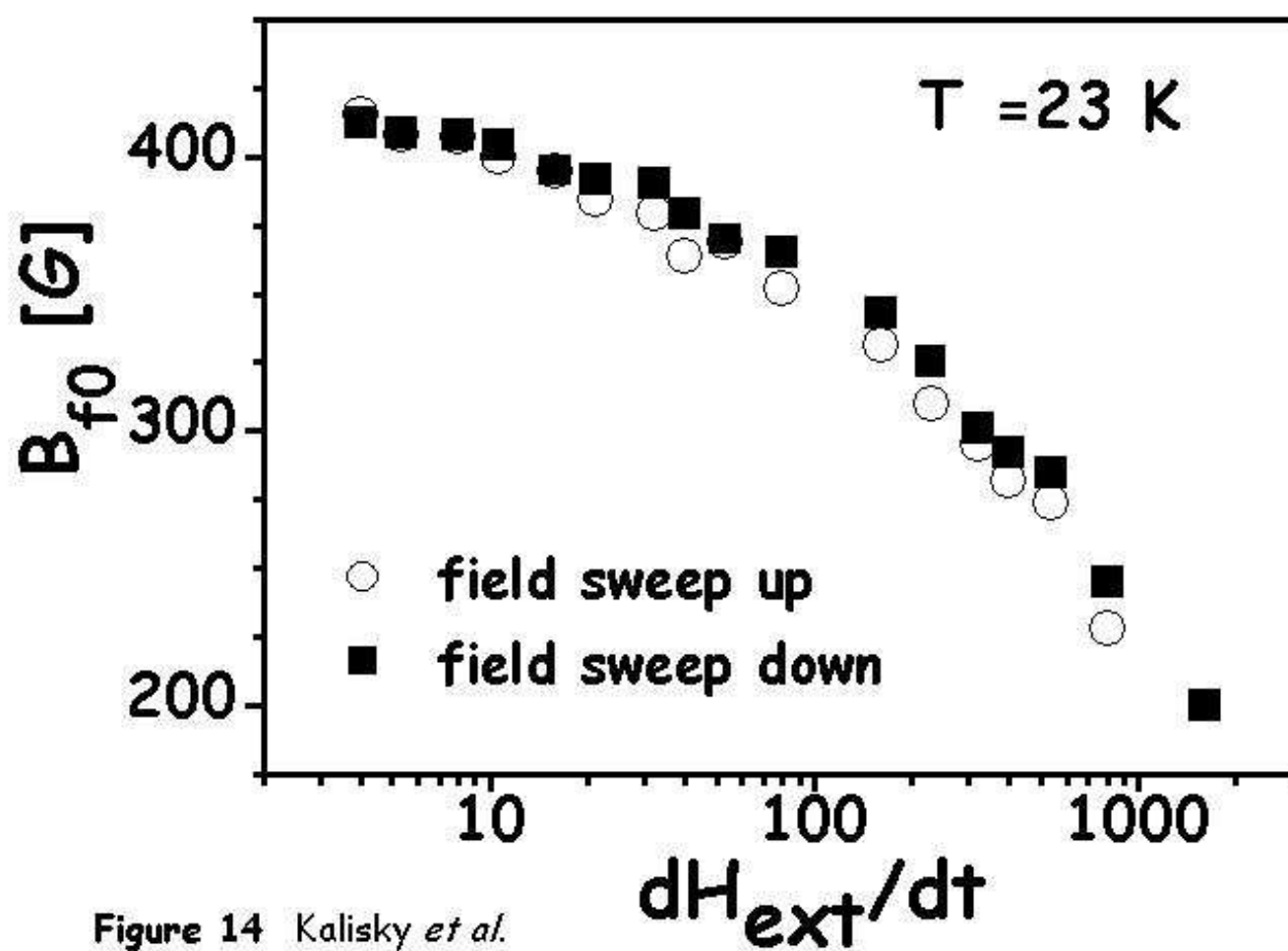


Figure 14 Kalisky *et al.*

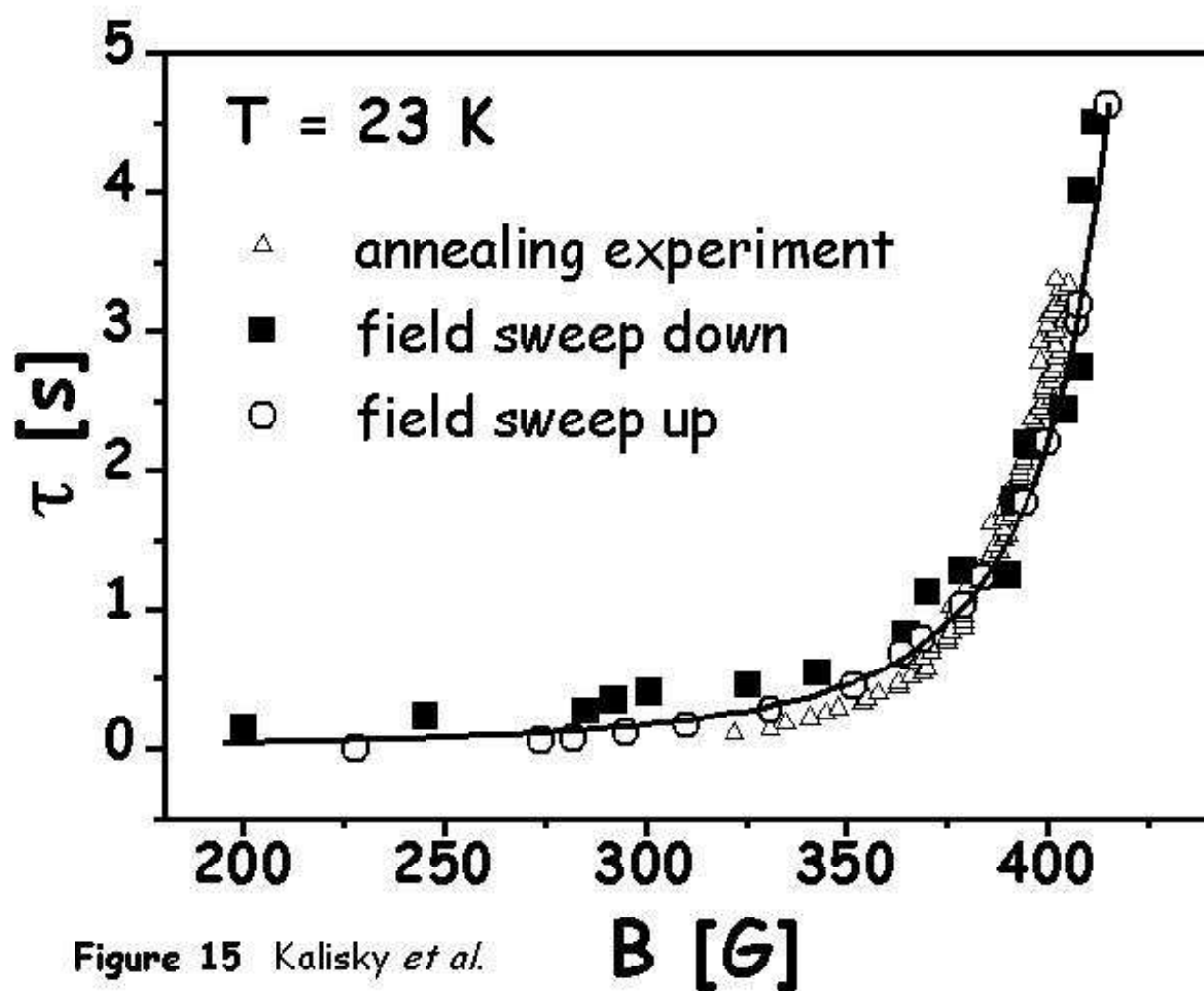


Figure 15 Kalisky *et al.*

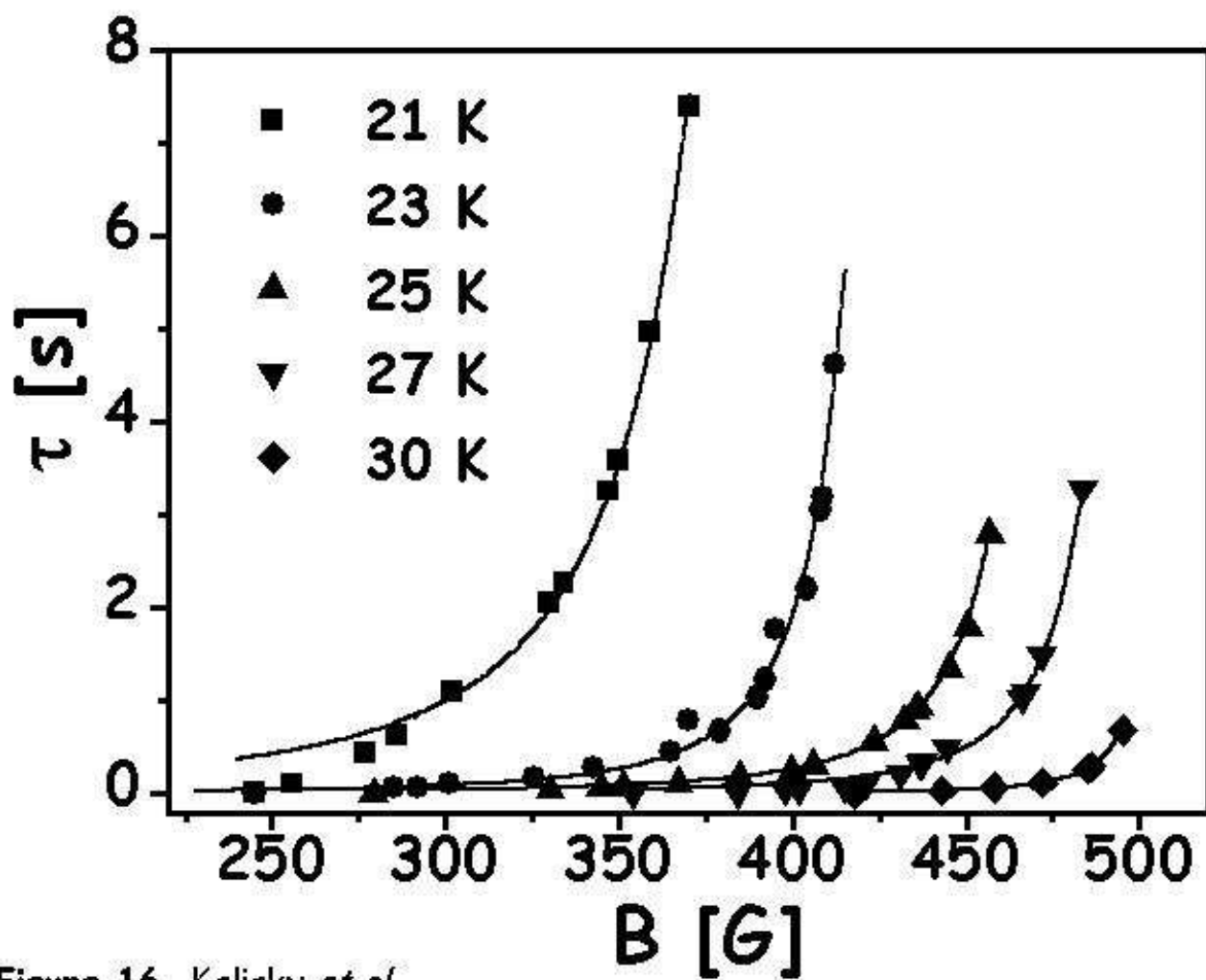


Figure 16 Kalisky *et al.*

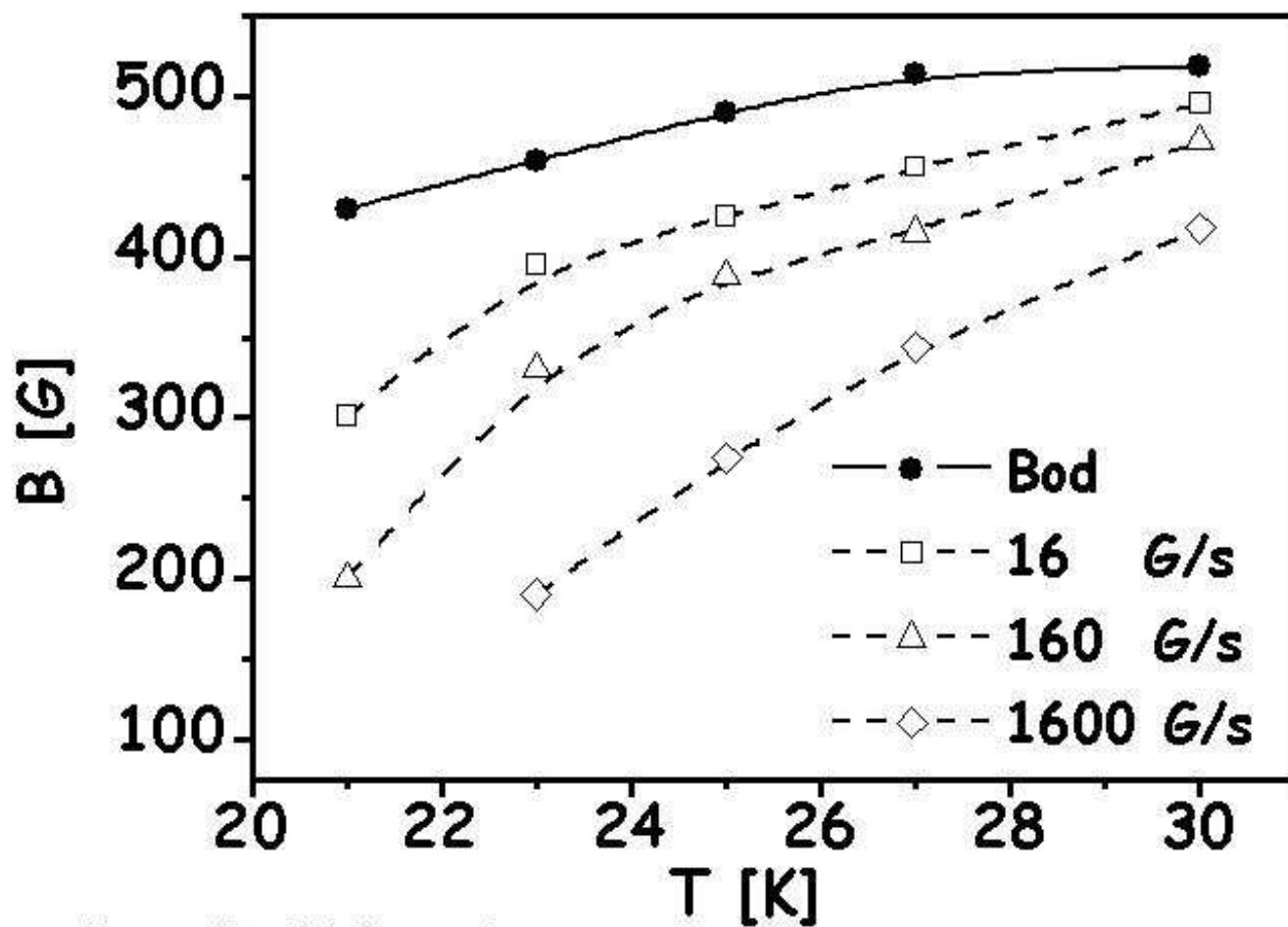


Figure 17 Kalisky *et al.*

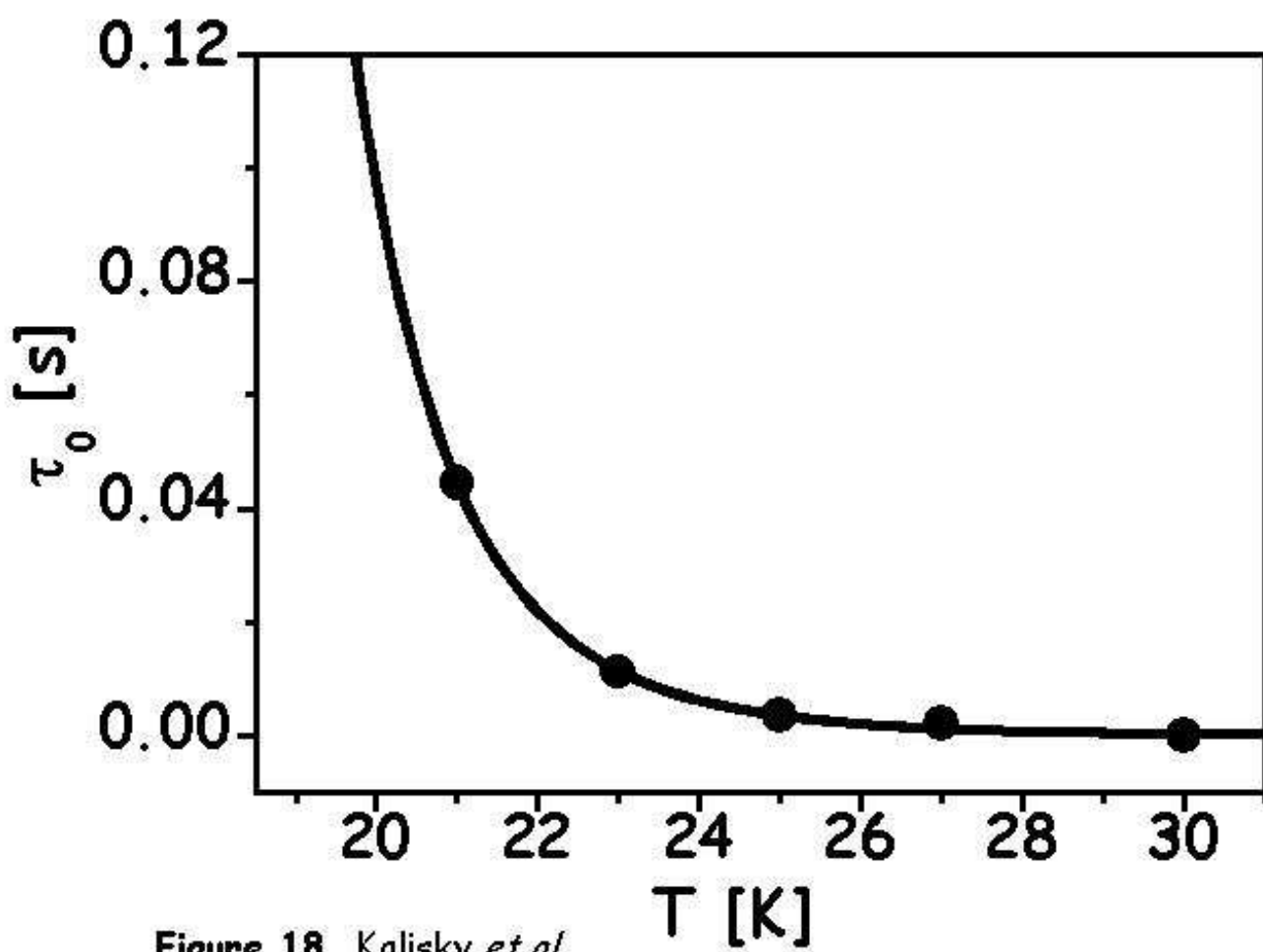


Figure 18 Kalisky *et al.*